Improved error estimates of a discharge algorithm for remotely sensed river measurements: Test cases on Sacramento and Garonne Rivers

Yeosang Yoon[1,2], Pierre-André Garambois[3], Rodrigo C.D. Paiva[4], Michael Durand[5], Hélène Roux[6], and Edward Beighley[1]

[1]Department of Civil and Environmental Engineering, Northeastern University, Boston, Massachusetts, USA, [2]Now at Sierra Nevada Research Institute, University of California, Merced, Merced, California, USA, [3]ICUBE- UMR 7357, Fluid Mechanics Team, INSA Strasbourg, Strasbourg cedex, France, [4]Instituto de Pesquisas Hidráulicas IPH, Universidade Federal do Rio Grande do Sul UFRGS, Porto Alegre, Brazil, [5]School of Earth Sciences, The Ohio State University, Columbus, Ohio, USA, [6]Université de Toulouse; INPT, UPS, CNRS; IMFT (Institut de Mécanique des Fluides de, Toulouse); Allée Camille Soula, Toulouse, France

Abstract We present an improvement to a previously presented algorithm that used a Bayesian Markov Chain Monte Carlo method for estimating river discharge from remotely sensed observations of river height, width, and slope. We also present an error budget for discharge calculations from the algorithm. The algorithm may be utilized by the upcoming Surface Water and Ocean Topography (SWOT) mission. We present a detailed evaluation of the method using synthetic SWOT-like observations (i.e., SWOT and AirSWOT, an airborne version of SWOT). The algorithm is evaluated using simulated AirSWOT observations over the Sacramento and Garonne Rivers that have differing hydraulic characteristics. The algorithm is also explored using SWOT observations over the Sacramento River. SWOT and AirSWOT height, width, and slope observations are simulated by corrupting the "true" hydraulic modeling results with instrument error. Algorithm discharge root mean square error (RMSE) was 9% for the Sacramento River and 15% for the Garonne River for the AirSWOT case using expected observation error. The discharge uncertainty calculated from Manning's equation was 16.2% and 17.1%, respectively. For the SWOT scenario, the RMSE and uncertainty of the discharge estimate for the Sacramento River were 15% and 16.2%, respectively. A method based on the Kalman filter to correct errors of discharge estimates was shown to improve algorithm performance. From the error budget, the primary source of uncertainty was the a priori uncertainty of bathymetry and roughness parameters. Sensitivity to measurement errors was found to be a function of river characteristics. For example, Steeper Garonne River is less sensitive to slope errors than the flatter Sacramento River.

1. Introduction

Methods for river discharge estimation by satellite remote sensing can be classified broadly into two types: (1) using hydraulic variables (e.g., channel width w, water surface elevation h and slope S, and cross-sectional area A) through a flow law relationship [e.g., *Smith et al.*, 1996; *Kouraev et al.*, 2004; *Bjerklie et al.*, 2005; *LeFavour and Alsdorf*, 2005; *Alsdorf et al.*, 2007; *Gleason et al.*, 2014, *Gleason and Smith*, 2014]; and (2) coupling satellite data to a hydraulic model [e.g., *Bates et al.*, 2006; *Andreadis et al.*, 2007; *Neal et al.*, 2009; *Biancamaria et al.*, 2011; *Yoon and Beighley*, 2015]. But no existing sensor can measure all desired hydraulic variables, which leads to difficulties in establishing a direct relationship between hydraulic variables and river discharge, or to construct a hydraulic model of the river system.

The Surface Water and Ocean Topography (SWOT) is an upcoming satellite mission, which will provide h and water surface extents using a Ka-band Radar Interferometers (KaRIN). With these observations, SWOT will provide terrestrial water storage changes and information for characterizing river discharge at global scales [*Durand et al.*, 2010b; *Rodríguez*, 2015; *Pavelsky et al.*, 2014]. While SWOT observations will be used in numerous scientific applications, there are two significant uncertainties in SWOT discharge estimation. First, direct SWOT observations will not provide all the information necessary for evaluation of the flow laws utilized, to date. Hydraulic geometry approaches relating river width and discharge require the coefficient and exponent to be calculated; a solution to this problem was recently presented by *Gleason and Smith* [2014].

In the context of Manning's equation, full channel bathymetry or roughness coefficient is necessary for discharge calculation. SWOT will directly measure water surface elevation at every overpass, observing changes in river depth above the level of the lowest-water elevation overpass, but the depth (or cross-sectional area) of river below the lowest observed elevation will remain unknown. In such context, several studies have developed discharge estimation methods from synthetic SWOT observations considering unknown bathymetry [e.g., *Durand et al.*, 2008, 2010a; *Yoon et al.*, 2012; *Mersel et al.*, 2013]. *Durand et al.* [2010a] found that bathymetry could be retrieved on the Ohio River only for river sections with significant surface slope variations. In that study, river width was temporally invariant in all cases, as rectangular channels were assumed. The second source of uncertainty in discharge estimates is the measurement errors of the SWOT observations, such as h, w, and S.

Durand et al. [2014] developed a Bayesian algorithm to estimate the unknown bathymetry, roughness coefficient, and lateral inflows and calculate discharge given SWOT observables. Conceptually, it was an extension of *Durand et al.* [2010a], but with the assumption of rectangular channels being relaxed, and by formally introducing prior information. The method of *Durand et al.* [2014] was successfully validated through examining the in-bank (discharge error of 10%) and out-of-bank (discharge error of 19%) scenarios for the River Severn (United Kingdom) using real in situ and remote sensing observations as a proxy for SWOT. In that study, however, river width was not observed and the method was not developed to handle the uncertainty of river width observations.

This study further develops the approach of *Durand et al.* [2014] using synthetic SWOT-like measurements. Specifically, discharge algorithm performance on two test case rivers, i.e., Sacramento (United States) and Garonne (France) Rivers, with different hydraulic characteristics is explored. Simulated airborne instrument AirSWOT measurements were used both test sites and SWOT observations were applied to an experiment for the Sacramento River Basin. AirSWOT will be utilized for SWOT calibration/validation, as well as to explore SWOT science questions prior to launching the satellite. In this study, we focus on characterizing discharge algorithm performance with simulated AirSWOT observations. Additionally, these experiments support proposed AirSWOT campaigns for the Sacramento and Garonne Rivers. In this study, the discharge algorithm was further developed to handle uncertain width observations and to improve the accuracy of the final estimates using Kalman filter. Furthermore, a discharge error budget is presented, and we show a way to partition uncertainty in the final discharge estimates between observations and the unknown bathymetry and roughness coefficient. Finally, the sensitivities of the algorithm accuracy to the uncertainty in SWOT-like measurements of river height, width, and slope are explored.

## 2. Study Area and Data

2.1. Sacramento River

The Sacramento River is the largest river by discharge in California, which is 640 km long and drains 72,000 km^2 in the northern end of the Central Valley [*Benke and Cushing*, 2005]. The Sacramento River basin has a broad range of altitude from 4000 m mean sea level (MSL) to 0 m MSL as the basin covers part of the Coast Ranges and the Sierra Nevada and discharges into the California Bay Delta. The climate in the Sacramento basin is varied due to the landforms. Average annual precipitation is 900 mm/yr, but that is mostly concentrated between November and March. The annual average flow is 657 m^3/s. The study area, situated in the upper Sacramento River, is about 40 km of flow length on the Sacramento River between the Colusa and Tisdale Bypass (Figure 1a).

An observation system simulation experiment was conducted to evaluate discharge algorithm performance. We used an one-dimensional (1-D) unsteady state HEC-RAS model (version 4.1) of the Sacramento River developed by the U.S. Army Corps of Engineers and the U. S. Geological Survey (USGS) as a synthetic true estimate of the hydraulic variables of the system. The model was calibrated using in situ data from a 2006 event. In this study, we tried to determine reach-averaged discharge rather than computing discharge at each cross-section, similar to *Durand et al.* [2014]. The river was split into seven reaches, each about 5–6 km in length. The reach-averaged quantities of height and slope were calculated based on the average of the polynomials obtained from a piecewise-linear representation of the water height. The reach-averaged widths were simply used as an average value for each reach.
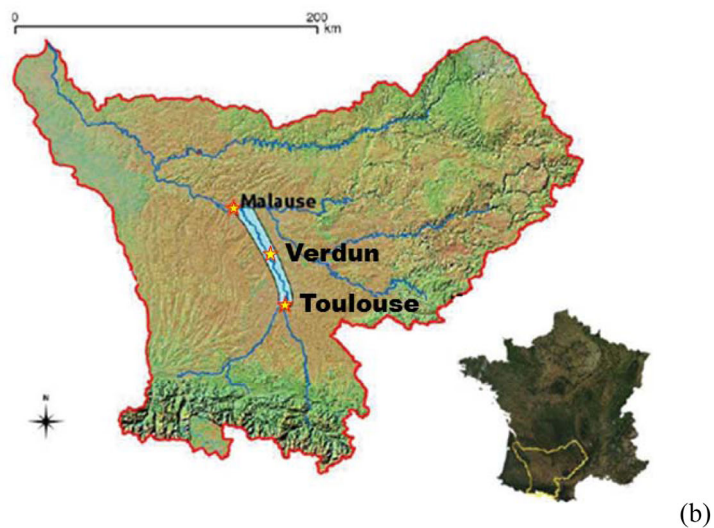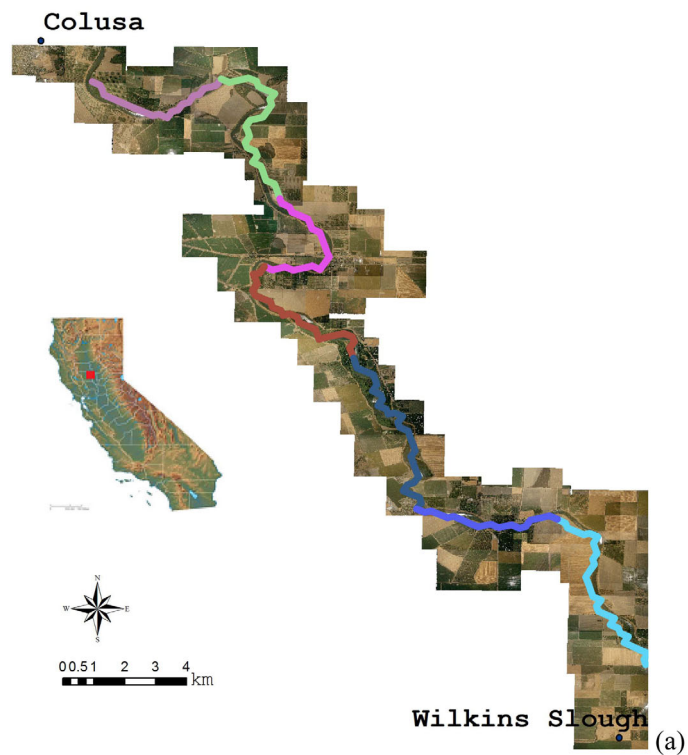
Figure 1. Map of Study area: (a) Sacramento River and (b) Garonne River.

Simulated both AirSWOT and SWOT observations of the Sacramento River are used to evaluate the discharge algorithm. Daily AirSWOT synthetic observations of river height, slope, and width were simulated from the reach-averaged quantities of the HEC-RAS model by adding zero-mean Gaussian random measurement errors (Figures 2a, 2c, and 2e). A 10-day simulation representing a 2-year flood scenario was used (in-bank and out-of-bank flow conditions). The river surface typically has a relatively low slope of 4.6 cm/km. Table 1 presents a summary of hydraulic characteristics. The SWOT instrument error are derived from several sources, such as random error, systematic error, and atmospheric propagation delays. In this study, we, however, simply considered the expected measurement errors of height, width, and slope to focus on evaluating the sensitivities of the algorithm accuracy to the uncertainty in measurements. Future work will address other errors. Nominal values of AirSWOT measurement errors of height, width, and slope were
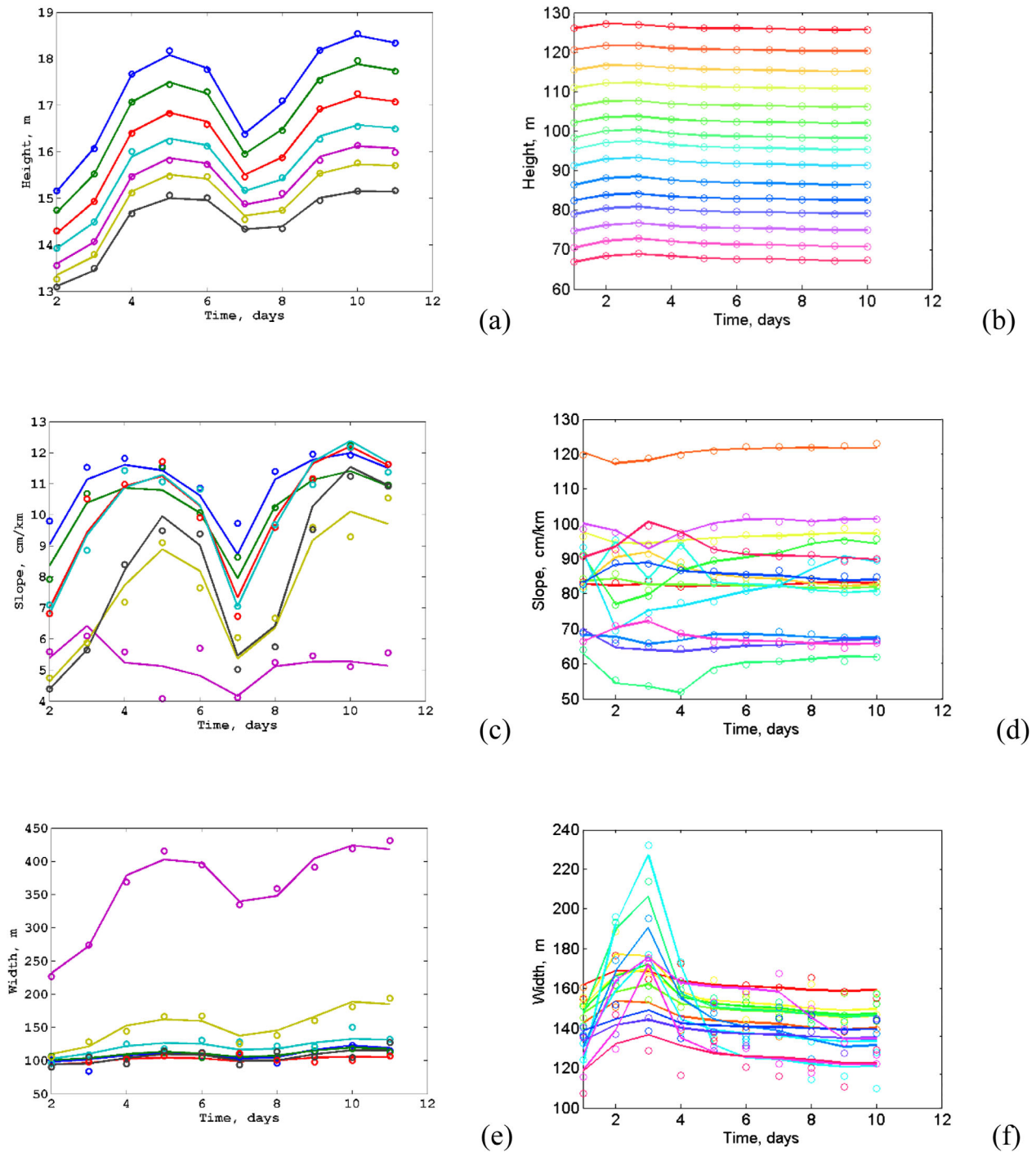
Figure 2. Reach averaged AirSWOT observations of height, slope, and width (circles) with true (solid lines) for (left) Sacramento River and (right) Garonne River.

applied as 5 cm, 7% of the width, and 0.55 cm/km, respectively [see *Moller and Carswell*, 2009 for details]. Sensitivity to these assumptions is evaluated in depth, herein. The SWOT observations were similarly simulated by the HEC-RAS hydraulic modeling results with the instrument error. While the HEC-RAS model structures and assumptions are the same as doing for the AirSWOT experiment, USGS gage measurements (#11389500, 1 February to 4 July 2009) were used as boundary inflows rather than 2-year flood dataset. The SWOT swath coverage of 140 km and 22-day revisit cycle were calculated, following previous work [see *Durand et al.*, 2010a; *Yoon et al.*, 2012, 2015 for details]. The expected SWOT measurement errors of height, width, and slope were applied as 10 cm, 15% of the width, and 1 cm/km, respectively.

Table 1. Summary of Hydraulic Characteristics of the Sacramento and Garonne Rivers

		Sacramento River	Garonne River
Length (km)		40	82
Reaches length (km)		5–6	5–6
Number of reaches		7	15
Width	Mean (m)	152	147
	Range	54 m (35%)	35 m (24%)
Slope	Mean (cm/km)	9	84
	Range	4.6 cm/km (52%)	8 cm/km (10%)
Height	Range (m)	2.73	1.88
Discharge	Mean (m^3/s)	760	401
	Range	597 m^3/s (79%)	440 m^3/s (110%)
Discharge per unit width	Mean (m^2/s)	5.00	2.72

2.2. Garonne River

The Garonne River drains an area of about 55,000 km^2 in France from its headwaters in the Spanish Pyrenees near the Pic d'Aneto to the Gironde estuary, where the mouths of the Garonne and the Dordogne merge. An 82 km reach of the Garonne River downstream of Toulouse is selected for this study (Figure 1b) with a drainage area of 10000 km^2 at Toulouse (upstream of the studied domain). The flow regime is highly variable, with low flows of ∼50 m^3/s in summer to large peak flows; the 2-year return period flood flow is 1400 m^3/s. The mean interannual discharge downstream Toulouse at Verdun s/Garonne gauging station is about 193 m^3/s (source: http://www.hydro.eaufrance.fr).

This river portion is studied in *Simeoni-Sauvage* [1999] and *Larnier* [2010]. The river morphology is described with 163 cross sections from *Simeoni-Sauvage* [1999], with cross-section spacing between 50 and 600 m. The river is rather steep with a mean slope of about 84 cm/km and its morphology is characterized by a quick succession of riffles and pools. A 1-D unsteady state HEC-RAS model was used. The model was calibrated between Toulouse and Malause, by comparing with *Larnier*, [2010], and its results will be used as a reference in the following. The studied domain is split into 15 reaches, each about 5-6 km in length. The reach-averaged quantities of height, width and slope were calculated same as the Sacramento case. A flood that occurred in January 2004 is used for this study. A uniform Manning roughness coefficient of 0.05 was calibrated resulting in a reasonably good agreement between the model and observations for the validation gauge of Verdun sur Garonne located in the middle of the study area. See Table 1 for a summary of the characteristics of the Garonne River test case.

The river domain is divided into 15 reaches of about 5-6 km length and cross-sectional data from the 1-D model are then reach averaged. Similar to the Sacramento River data, a 10-day simulation was performed. AirSWOT measurement errors are added as Gaussian random errors to the "true" values, using the same values noted above for the Sacramento (Figures 2b, 2d, and 2f).

3. Discharge Estimation Methodology

The goal of the method presented here is to estimate river discharge given SWOT-like observables, i.e., river height, slope, and width. First, the numerical equations for the river flow were formulated using the Manning's equation with continuity equation. Second, the optimal values of the unknown river hydraulic parameters (i.e., low-flow cross-sectional area A_0 and the roughness coefficient n) are estimated using a Bayesian Markov Chain Monte Carlo (MCMC) scheme. Finally, the river discharge is estimated using the Manning's equation with the optimal values of A_0 and n. Our method is explained in more detail below.

3.1. Governing Equations

The instantaneous river discharge from the SWOT mission can be estimated via the Manning's equation with substituting the SWOT observables. Here, we assumed that channel width is close to the wetted perimeter and water surface slope is equal to the friction slope. The equation is given by:

$$Q = \frac{1}{n}(A_0 + \delta A)^{5/3} w^{-2/3} S^{1/2} \tag{1}$$

where n is the Manning's roughness coefficient, A_0 is the low-flow cross-sectional area, δA is the change in cross-sectional area corresponding to the A_0 (see section 3.2 for details), w is the top width of flow, and S is the water surface slope.

In equation (1), while δA, w, and S are derived from SWOT observations, A_0 and n are unknown a priori. The A_0 and n can be determined by several ways, but we have proposed a Metropolis algorithm in a Bayesian MCMC scheme where we derive A_0 and n directly from the SWOT observations, based on the diffusive approximation of the 1-D Saint-Venant equations. The mass and momentum conservation equations are simply given by:

$$\frac{\partial Q}{\partial x} + \frac{\partial A}{\partial t} - q = 0 \tag{2a}$$

$$S_f = -\frac{\partial h}{\partial x} - \frac{V}{g}\frac{\partial V}{\partial x} - \frac{1}{g}\frac{\partial V}{\partial t} \tag{2b}$$

where Q is the discharge, x is the flow distance along the channel, A is the flow cross-sectional area, t is the time, q is the lateral inflow, S_f is the friction slope, h is the water surface elevation, V is the velocity, and g gravity. On the right-hand side of equation (2b), the third two terms are advection and acceleration that may be neglected here for large rivers.

3.2. Flow Cross-Sectional Area
SWOT will provide h and the corresponding width w that can be used to estimate a cross-sectional flow area. We represent the cross-sectional area as the sum of the cross-sectional area on the first observation day A_0 and the change in cross-sectional area δA. The latter can be written as integrals of w over h. Thus, the cross-sectional area is defined by:

$$A(h) = A_0 + \delta A = A_0 + \int_{h_{min}}^{h} w(h')dh' \tag{3}$$

The δA is evaluated using trapezoidal integrals over the time-series of the SWOT measurements. The equation is written as:

$$\delta A(r,t) = \sum_{i<t} dA_{r,i} \tag{4}$$

where r indicate reach, dA is the change in cross-sectional area during the period from t to $t+1$:

$$dA(r,t) = \int_{h_t}^{h_{t+1}} w(h')dh' \approx \frac{w(r,t+1)+w(r,t)}{2}[h(r,t+1)-h(r,t)] \tag{5}$$

3.3. Integrating Mass Conservation Equation to SWOT Observations
In this study, we integrated the mass conservation equation (equation (2)) between two overpasses separated by Δt and discretized the spatial flow derivative using a finite difference. The vector form of the resulting mass balance equation is shown:

$$\Delta_x \mathbf{Q} + \Delta_t \mathbf{H} \cdot \mathbf{BW} = \mathbf{q} \tag{6}$$

where Δ_x is derivative of flow imbalance, $\mathbf{Q}$ is the flow imbalance term, Δ_t is derivative of time, $\mathbf{H}$ is the water surface elevation, $\mathbf{B}$ is the operational matrix for averaging the channel width, $\mathbf{W}$ is the vector form of the top width, and $\mathbf{q}$ is the vector form of the lateral inflow. The detailed derivation of the equation refers to Appendix A in *Durand et al.* [2014].

We then can define the error of the flow routing equation, Θ from equation (6) as below:

$$\Theta = \Delta_x \mathbf{Q} + \Delta_t \mathbf{H} \cdot \mathbf{BW} - \mathbf{q} \tag{7}$$

The unknown A_0 and n are embedded in flow imbalance term $\mathbf{Q}$ via equation (2) and the A_0 and n can be estimated by minimization of the Θ. The dimension of Θ is $n_\Theta \times 1$, where $n_\Theta = n_R(n_t - 1)$, where n_R is the

number of reaches and n_t is the number of overpasses. Assuming that A_0 and n are unknown and vary in space, and $\mathbf{q}$ is known and assumes zero; thus there would be $2n_R$ unknowns in the Θ.

3.4. Bayesian Approach

The Bayesian approach is used here to infer estimates of unknown parameters, A_0 and n, combined with the prior information based on SWOT observables. In this study, we assumed that $\beta=[A_0, n]$ is the unknown vector and $\alpha=[h, w, S]$ is the vector of the observations in space and time. Thus, the goal of the Bayesian approach is to estimate β given α. The form of the Bayes' theorem is given by:

$$p(\beta|\alpha) \propto p(\alpha|\beta)p(\beta) \tag{8}$$

where $p(\beta|\alpha)$ is the posterior probability density function (PDF), $p(\alpha|\beta)$ is the likelihood function, and $p(\beta)$ is the prior information on β. The Θ is a function of both α and β. The Bayesian approach was developed, following *Durand et al.* [2014] that describes the detailed equations.

For the Sacramento River, the prior values of the unknown parameters A_0 and n were simply assumed as $A_0 \sim N(300, 200)$ and $n \sim N(0.03, 0.01)$ considering the worst-case scenario. This first guess of A_0 and n underestimates true values by 49% and 11% with 67% and 33% uncertainties, respectively. Similar to the Sacramento case, the prior values of A_0 and n for the Garonne River also underestimated the true values by an average of 21% and 20% with 35% and 20% uncertainties, respectively.

3.5. Markov Chain Monte Carlo (Metropolis Algorithm)

The MCMC method is addressed to find "the best" estimate of unknown parameters A_0 and n with an acceptable error because it can practically be impossible to find the right answer directly, given the probability distribution. The MCMC technique provides a large number of sampling opportunities from the probability distribution, which can lead to convergence of the stationary results. The Metropolis algorithm [*Metropolis et al.*, 1953] is a popular and simple algorithm for the MCMC method, which is used to address a Markov chain on the parameter β for this study. The Metropolis algorithm is started with an arbitrary initial value β^0 (i.e., first guess) of β. New candidates are sequentially generated by repeating the following cycle, with $\{\beta^s|\beta^{s-1} : s=1, 2, \ldots\}$ that is generated from a Markov Chain. First, the new candidate β^* is proposed as a "jump" distribution and evaluate the new unnormalized posterior $p(\beta^*|\alpha)$. Second, the acceptance probability is calculated to decide whether or not to accept the new candidate.

$$r = \frac{p(\beta^*|\alpha)}{p(\beta^{s-1}|\alpha)} \tag{9}$$

The new candidate β^* is accepted if r is larger than η that is a uniform random variable between 0 and 1 (i.e., $\eta \in [0, 1)$). The acceptance ratio (i.e., jumping rule) is a critical factor for the efficiency of the algorithm. Here, we select acceptance rates around 0.25, following *Gelman et al.* [1996]. Finally, the estimates of A_0 and n from the Bayesian MCMC scheme were used to estimate river discharge $\hat{\mathbf{Q}}$ for the Markov chain via equation (1).

3.6. Improving the Discharge Estimates Using the Kalman Filter

Note that discharge is not estimated *per se* as part of the MCMC; instead, the MCMC estimates the A_0 and n parameters. The parameters are then used with the noisy observations to estimate discharge. This leads to situations where e.g., mass conservation is not strictly conserved between reaches. For example, when the river channel is wide and shallow, the slope observations may be simulated close to zero due to observation error (see Figure 2). In this case, the discharge estimates from Markov Chain show a poor performance. The abrupt change in the hydraulic characteristics can also lead to increased error. To solve this problem, we simply added a post-facto Kalman filter technique on the discharge estimates from Markov Chain.

The Kalman filter analysis equation for the update is:

$$x^+ = x^- + K(y - Fx^-) \tag{10}$$

where x^+ is the posterior state estimate (or analysis) and x^- is the prior state estimate (or forecast); the prior estimate is derived from the estimates of the Metropolis algorithm $\hat{\mathbf{Q}}$. y is the observations, which is defined by rearranging equation (6):

$$y = \Delta_{\mathbf{t}} \mathbf{H} \cdot \mathbf{BW} \tag{11}$$

F is the operation operator that is needed to linearly relate y and $\bar{x}$; note $F = -\Delta_{\mathbf{t}}$. K is the Kalman gain that is given by:

$$K = PF^{T}[FPF^{T} + R]^{-1} \tag{12}$$

where prior error covariance P, here, is defined as a variance of the $\hat{\mathbf{Q}}$, R is the observation error covariance, defined as:

$$R = J_{\bar{A}} C_{\alpha} J^{T}_{\bar{A}} \tag{13}$$

where $J_{\bar{A}}$ is the partial derivatives of $\Delta_{\mathbf{t}} \mathbf{H} \cdot \mathbf{BW}$ in equation (7) with respect to height and width and C_{α} is observation covariance matrix that is calculated independence between height, width, and slope errors.

3.7. Discharge Error Budget

We approximated the error budget of the discharge estimates $\hat{\mathbf{Q}}$ using all inputs to the Manning's equation (see equation (1)). This is given by:

$$\sigma_{Q}^{2} \approx J \sum_{x} J^{T} \tag{14}$$

where x is all inputs to the Manning's equation; note $x = |\hat{\mathbf{n}} \quad \hat{\mathbf{A}}_{\mathbf{0}} \quad \delta A \quad w \quad S|$, J is the Jacobian of the $\hat{\mathbf{Q}}$ and $\sum_{x}$ is the covariance matrix of all inputs to the Manning's equation. Ideally, we should determine covariance between the parameters and observations, but we only considered, here, a correlation between parameters A_0 and n. Other covariances among the observations were ignored. Substituting in the partial derivatives of $\hat{\mathbf{Q}}$ and arranging the equations, the error budget of the $\hat{\mathbf{Q}}$, U($\hat{\mathbf{Q}}$) is:

$$U(\hat{\mathbf{Q}}) \approx U(\hat{\mathbf{n}}) + U(\hat{\mathbf{A}}_{\mathbf{0}}) + U(\hat{\mathbf{A}}_{\mathbf{0}}\hat{\mathbf{n}}) + U(w) + U(S) = \left(\frac{\sigma_{\hat{\mathbf{n}}}}{\hat{\mathbf{n}}}\right)^{2} + \left(\frac{5}{3}\frac{\sigma_{\hat{\mathbf{A}}_{\mathbf{0}}}}{\hat{\mathbf{A}}_{\mathbf{0}} + \delta A}\right)^{2} - 2\rho \frac{5}{3}\frac{\sigma_{\hat{\mathbf{A}}_{\mathbf{0}}}\sigma_{\hat{\mathbf{n}}}}{(\hat{\mathbf{A}}_{\mathbf{0}} + \delta A)\hat{\mathbf{n}}} + \left(\frac{5}{3}\frac{\sigma_{\delta A}}{\hat{\mathbf{A}}_{\mathbf{0}} + \delta A}\right)^{2}$$
$$+ \left(\frac{2}{3}\frac{\sigma_{w}}{w}\right)^{2} + \left(\frac{1}{2}\frac{\sigma_{S}}{S}\right)^{2}$$
$$\tag{15}$$

where ρ is a correlation between A_0 and n. The σ is used in the equation to mean "standard deviation".

4. Results and Discussion

This study focuses on evaluating the potential to estimate river discharge using SWOT-like measurements. Here, we first characterized the expected discharge algorithm accuracy. For the Sacramento River, both simulated AirSWOT and SWOT observations were used. AirSWOT observations were utilized for the Garonne River. Then, we evaluated the sensitivity of the algorithm accuracy to the uncertainty in synthetic AirSWOT measurements of height, width, and slope for both test sites.

4.1. Discharge Algorithm Accuracy
4.1.1. Identification on the Sacramento River
4.1.1.1. AirSWOT Scenario

Figures 3a and 3c show estimates of low-flow cross-section area and roughness coefficient for each reach. It shows how the prior n and A_0 values converge to the true values after the estimation procedure. On average, the algorithm underestimated the true A_0 by 20%, reducing the error from the first guess by 41%. In particular, even though the prior A_0 estimates of the reaches 5, 6, and 7 have more than 50% relative error, the MCMC method was able to recover the A_0 values. The standard deviation of the posterior estimates (average across all reaches) is 68 m^2, which is 66% smaller than the prior uncertainty. Similarly to what is observed for the A_0 parameter, estimates of n follow the spatial pattern of the true values and the algorithm underestimated it by 14%. The standard deviation of the posterior estimate is 0.0045, which represents 14% of the average true value of n. Note that both the A_0 and n are underestimated in the Markov Chains (Figures 3a and 3c), but these errors were canceled out via the Manning's equation (i.e., equation (1)) resulting in an accurate discharge estimate.

Figure 4a shows the discharge estimates Q derived from Manning's equation using estimated values of A_0 and n, as well as AirSWOT observables (i.e., h, w, S, and δA). In the figure, the flow patterns of Q for reach 5
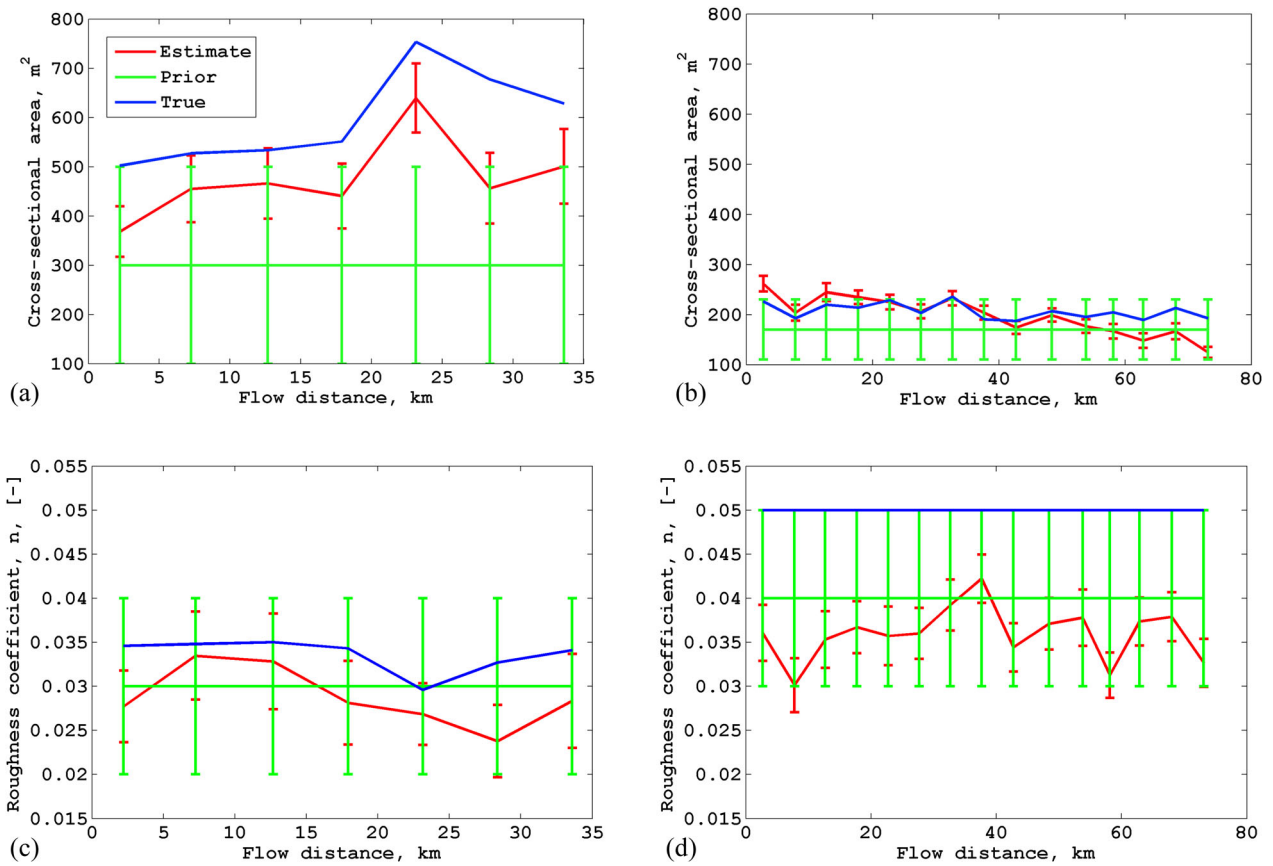
Figure 3. Estimation of (top) cross-section area and (bottom) roughness coefficient for each reach of both (left) Sacramento River and (right) Garonne River with expected AirSWOT measurement errors.

(Figure 4a, green line) is different from the other flows during day 5. Note that the channel width of reach 5 is much wider than the others, and it presents shallow slopes (almost close to zero) as well, which can lead to noise in estimating the discharge. Figure 4c presents an improved estimate of Q from Figure 4a using the Kalman filter. Discharge of reach 5 was successfully corrected via the Kalman filter. The other discharge estimates were also updated to be closer to the true Q. It is clear that the Kalman filter should be useful to improve the accuracy of the discharge estimates when the hydraulic characteristics are changed rapidly, as well as when the worst-case dataset was applied. On average, the algorithm underestimated the truth by 64 m^3/s (8.5%) and RMSE error was 68 m^3/s (9%).

Figure 5a presents the joint PDF of the A_0 and n derived from the Markov Chains for the first (upstream) reach, showing that the estimation scheme provided highly correlated A_0 and n values. Such results are to be expected, as from equation (1) it is easy to see the opposite effects of A_0 and n on discharge. Figure 5c shows discharge RMSE errors for the first reach as a function of the A_0 and n. These results demonstrate how several (A_0, n) pairs can produce similarly satisfactory discharge errors and that the best (A_0, n) values are encountered in a region of the parameter space surrounding a line defined approximately by the points (260 m^2, 0.019) to (560 m^2, 0.04).

The average Q uncertainty, calculated from uncertainty analysis (equation (14)), is 16.2%. Figure 6 presents the discharge error budget. The error budget is almost entirely dominated by the uncertainty of A_0 and n; 81% of error variance is explained by A_0 and n. The sensitivity of this error budget to AirSWOT observation uncertainty is presented in section 4.2.

4.1.1.2. SWOT Scenario

The accuracy of the Bayesian MCMC approach is evaluated using SWOT observations. During the experimental period, 21th SWOT observations (three times (day-5, 8, and 20) per 22-day repeat cycle) over seven reaches on the Sacramento River are measured (see Figure 7a), then the observations were used to
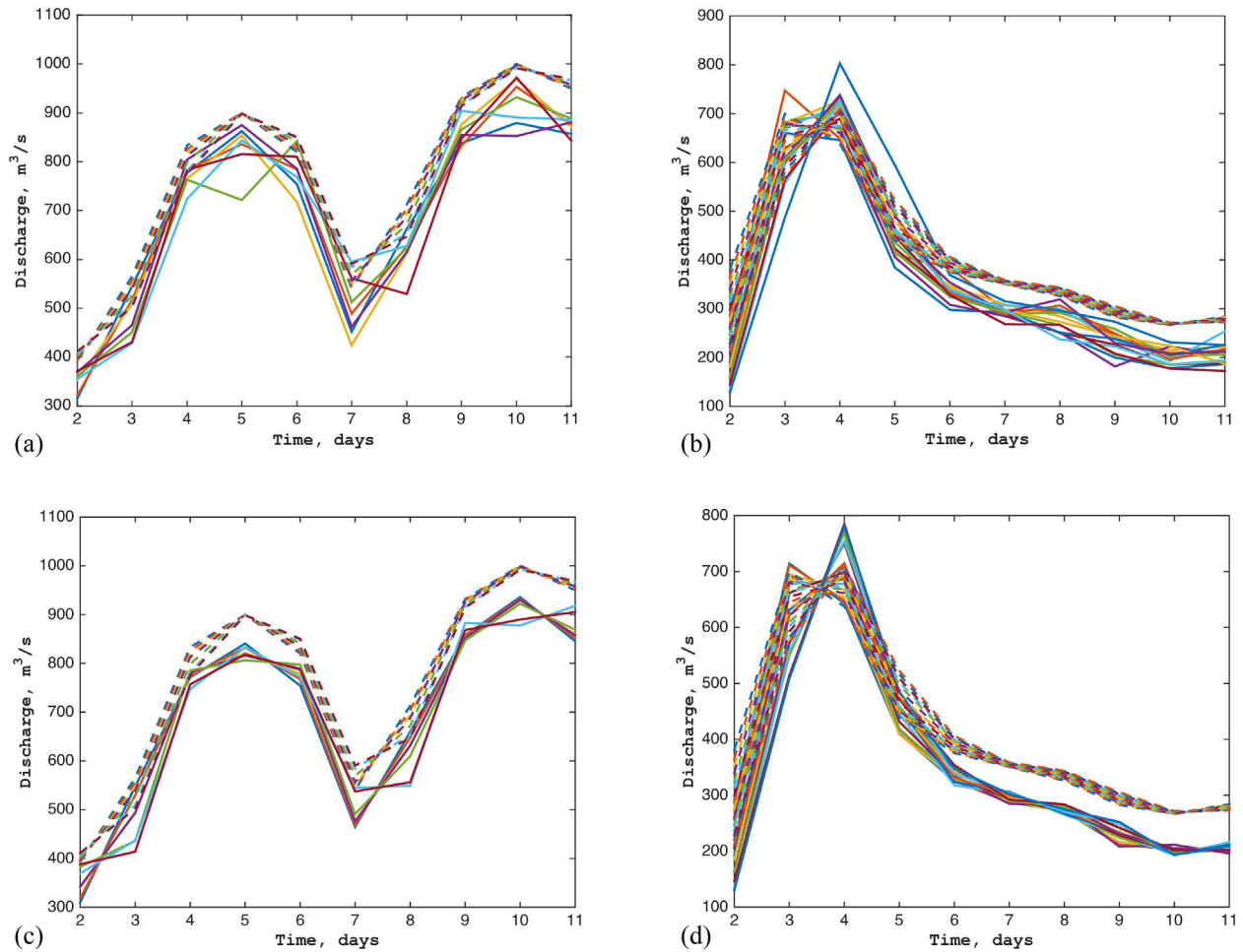
Figure 4. Hydrograph for 10 experimental days: (top) before filtering and (bottom) after filtering for (left) Sacramento River and (right) Garonne River. Dashed lines are "true" HEC-RAS model discharge and solid lines are estimated with the algorithm.

characterize the algorithm performance. The expected SWOT observational errors of height, width, and slope (10 cm, 15% of the width, and 1 cm/km, respectively) were applied. Similar to the AirSWOT case, prior estimates of A_0 and n were generated from the Gaussian random function; note $A_0 \sim N(200, 100)$ and $n \sim N(0.03, 0.01)$. That means the priors of A_0 and n were guessed and underestimated the truths by an average of 36% and 14% with 50% and 33% uncertainties, respectively.

Figure 7a shows the estimated hydrograph along with truth and SWOT observational time during the entire experimental period. Q temporal variations captured well over the experimental period, but the Q estimates do miss abrupt changes in days 20–40 that are days in between SWOT overpasses. Recent research tried to solve the temporal sampling issue of the SWOT mission using spatiotemporal interpolation technique [*Paiva et al.*, 2015; *Yoon et al.* 2013]. The error derived from the temporal resolution of the SWOT is not considered in this study due to the focus on the uncertainty of the SWOT observables; future work will address it. The Q uncertainty (error bars, Figure 7a) is estimated via standard deviation across the Markov chain. The uncertainty ranges from 24 m^3/s (30%) at lowest flow to 126 m^3/s (18%) at peak flow. The absolute uncertainty and relative uncertainty shows the opposite results because the unknown parameters A_0 and n less important at high flow. Figure 7b shows the estimated hydrograph with truth at times when SWOT observations are available. While Q estimates capture the flow pattern well, the Q estimates at low flow period underestimated the truths. Overall, the mean RMSE error of the estimated Q is 40 m^3/s (15%) and average Q uncertainty is 16.2%.

4.1.2. Identification on the Garonne River
The identification of the low-flow cross-section area and roughness coefficient for each reach of the Garonne River is shown in Figures 3b and 3d. For all the reaches, the mean absolute relative error on A_0 is
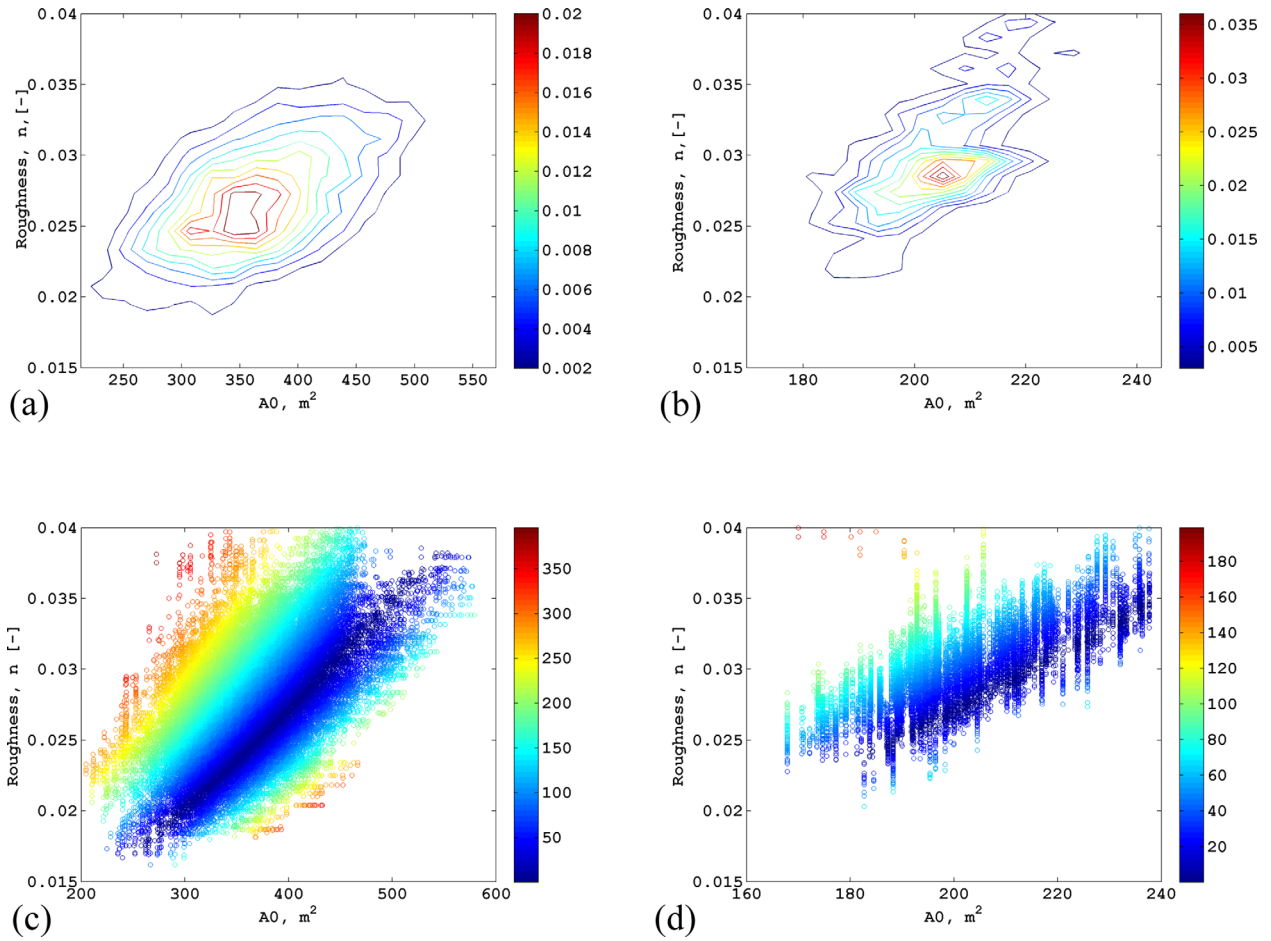
Figure 5. (top) Projection of the joint PDF and (bottom) discharge RMSE from the Markov chain in the parameter space of A_0 and n: (left) first reach of the Sacramento River and (right) second reach of the Garonne River. Color bars refer to discharge RMSE (m^3/s) and joint PDF of A_0 and n, respectively.

11.2% and 30% on n, which respectively represents 8.8% improvement and 10% deterioration compared to the first guess. The low-flow cross-sectional area A_0 is overestimated for the four first reaches and underestimated for the five last reaches. The roughness coefficient n is systematically underestimated with a mean spatial value of 0.036 against 0.05 for the reference value.

Figure 4b shows the estimated discharge of each reach. Overall, discharge estimates are in reasonably good agreement with peak flow but systematically underestimates flood recession. The (n, A_0) couples identified with the algorithm are equivalent roughness geometry couples [cf. *Garambois and Monnier*, 2015] producing discharge with a 15.2% RMSE averaged in space. An improved estimate of discharge using the Kalman filter is presented in Figure 4d. Using this technique to correct discharge estimate afterward tends to narrow the spreading of discharge estimates, but the improvement was limited compared to the Sacramento River case.

Similar to the Sacramento case, Figure 5b presents the joint PDF of the A_0 and n derived from the Markov Chains for the second (upstream) reach, showing that the estimation scheme provided highly correlated A_0 and n values. The discharge RMSE in m^3/s is projected in the (A_0, n) plane (Figure 5d) for the reach 2. Several plausible (A_0, n) couples producing good RMSE on discharge are located in a quasi-linear set of the parameter space, spanning from (190 m^2, 0.025) to (240 m^2, 0.035). Those equivalent roughness geometry couples result in comparable performances averaged in space on discharge. As expected there is for each reach an infinity of plausible (A_0, n) couples, lying on a line in the dark blue region. Note that in the case of the Garonne River, the parameter space is less sampled than for the Sacramento. As an account of inverse model hypothesis and measurement errors, the algorithm can approach a feasible solution but never reach the true (or true-equivalent) hydraulic behavior of the study domain.
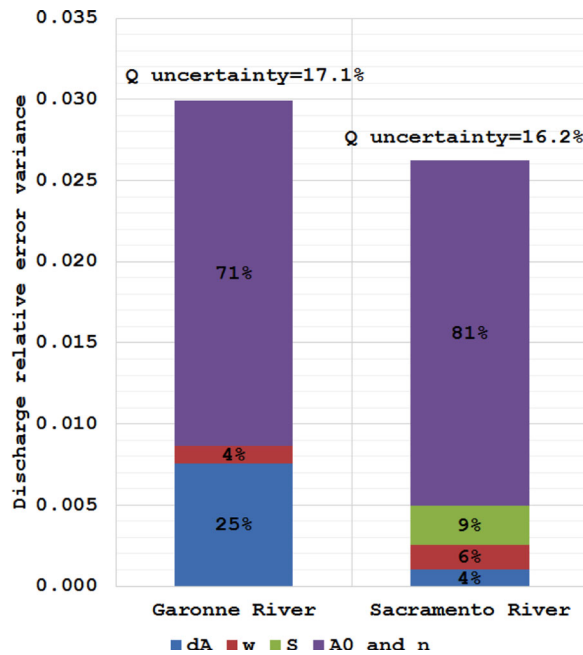
Figure 6. AirSWOT discharge error budget from Manning's equation.

The mean RMSE error of discharge is 15.2% while the average uncertainty is 17.1% and the error budget with respect to the Manning equation is represented in Figure 6. Discharge uncertainty is dominated by two components: 71% of the variance is explained by (n, A_0) and 25% by the error on δA, while only 4% of the variance is due to observation errors on width and slope.

4.2. Sensitivity of the Algorithm Accuracy to the Uncertainty in AirSWOT Measurements

We demonstrated in the previous section how SWOT observations can be used to calculate discharge estimates on two rivers. For both rivers, we presented a single case, in which the observation uncertainty was specified. In this section, we evaluate the sensitivity of the algorithm accuracy, subject to changing uncertainty in the observables, such as height, width, and slope. The priors of A_0 and n, as well as the MCMC iteration length, are identical to that used in section 4.1.

4.2.1. Sacramento River

Figure 8a shows the results of the sensitivity of discharge uncertainty in the Sacramento River (as calculated via equation (15)) to height measurement errors. Here, height error is increased from 1 to 25 cm, while width and slope errors are fixed as 7% of the width and 0.55 cm/km, respectively. In Figure 8a, the green triangles represent the overall discharge uncertainties. At a height error of 5 cm (what we expect from AirSWOT), the discharge uncertainty is 16.2%. As the height error increase to 10 cm, there is little or no change in the discharge uncertainty. As the height error increases to 25 cm, the discharge uncertainty increases to nearly 30%. Thus, the uncertainty in A_0 and n is governed by the width and slope error for height errors less than 10 cm. The error budget can be broken down to show uncertainty due to unknown parameters, and that due to observations. In Figure 8a, the blue diamonds and red squares show the breakdown in the uncertainty of the unknown parameters A_0 and n, and observations, respectively. The observation error is uniformly a smaller part of the error budget. As the height error increases past 10 cm, there is a clear increase in the discharge error from 8% to 14%. However, the uncertainty in A_0 and n increased significantly from 18% to 26%. Thus, the main mechanism for increasing discharge uncertainty due to height error is the increase in the uncertainty of the unobserved parameters, A_0 and n. Figure 9a illustrates the uncertainty between unknown parameters and observations (note: uncertainty is presented as a variance in Figure 9). Figure 9a further illustrates the sensitivity of the Sacramento River discharge estimate to height error. Uncertainty due to unknown parameters always dominates.

Figure 8c shows the sensitivity to the slope errors. Here, we tested values ranging from 0.25 to 2.25 cm/km, while the height and width errors are fixed as 5 cm and 7% of the width, respectively. The expected slope error of the AirSWOT observations is between 0.55 and 1 cm/km. The uncertainty in discharge due to the observations (red squares) increases significantly as observation errors increase (Figure 8c). As the slope error increases past 1.2 cm/km, the error due to observations increased much more rapidly, while the error in A_0 and n did not increase. Figure 9c helps to visualize how the slope error takes over the discharge error budget when it increases much past 1.25 cm/km. For slope error of 2.55 cm/km, the discharge error budget is dominated by slope error, for the Sacramento River.

Figure 8e presents the sensitivity of the discharge uncertainty to the width error. Here, width error is increased from 2% to 30% of the nominal width while the height and slope error are fixed as 5 cm and 0.55 cm/km, respectively. The discharge uncertainty due to the width directly increased steadily, while the discharge uncertainty due to the uncertainty in A_0 and n increased more slowly. The breakdown of the
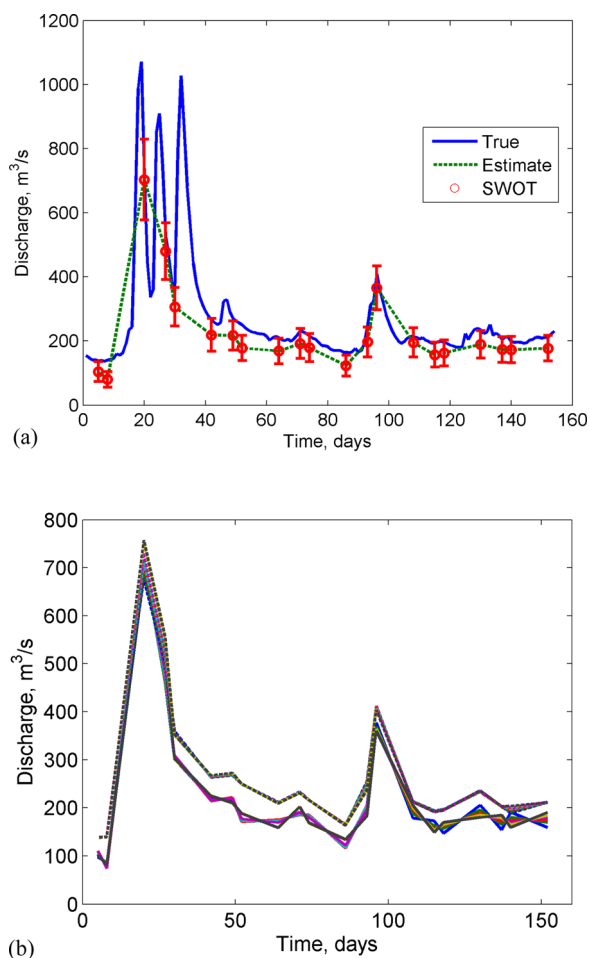
Figure 7. Hydrographs for the SWOT scenario: (a) reach-averaged discharge estimates along with truth and SWOT observational times and (b) estimated hydrograph with truth at times when SWOT observations are available. Dashed lines are "true" HEC-RAS model discharge and solid lines are estimated with the algorithm.
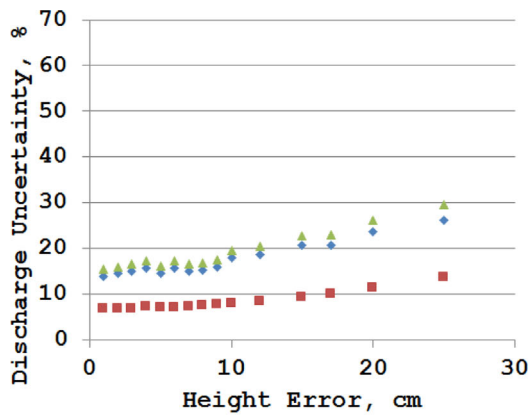
uncertainty of the unobserved parameters and observations are shown in Figure 9e. As the width error increases past 20%, the discharge error budget is dominated by the width error.

Note that the error budget on discharge is generally dominated by the uncertainty in A_0 and n, rather than the uncertainty of the Air-SWOT observations; note that A_0 and n were guessed with the worst-case scenario. As shown here, there is significant sensitivity to height, width, and slope errors due to the sensitivity of A_0 and n to measurement error. Based on nominal values of observation uncertainty, doubling the width error, the slope error, or the height error all lead to approximately a discharge uncertainty near 20%, and about 10% uncertainty due to the observations. Thus, there is some space for AirSWOT observation uncertainty to be greater than the nominal values, and still achieve discharge uncertainty near 20%.
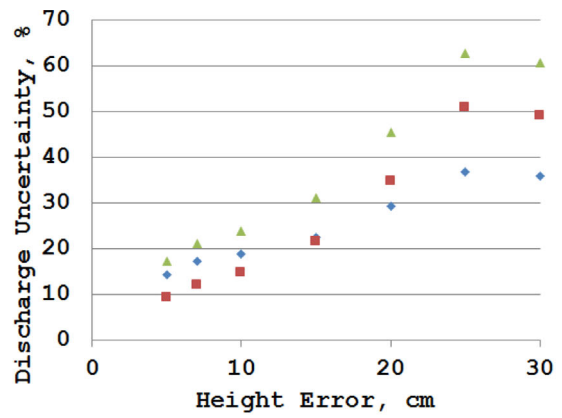
4.2.2. The Garonne River

The sensitivity of the algorithm to AirSWOT measurement errors is tested on the Garonne River. First the sensitivity of discharge estimation to height errors is tested as shown in Figure 8b, the green triangles representing the overall discharge estimation error. The discharge uncertainty increases significantly with height error, in contrast to the Sacramento River. At a height error of 5 cm, the discharge uncertainty is 17.1%. As the height error increases to 25 cm, the di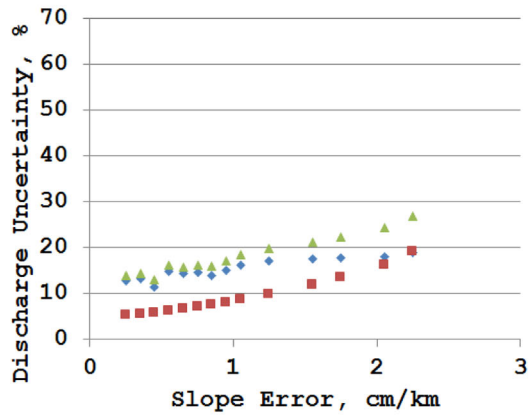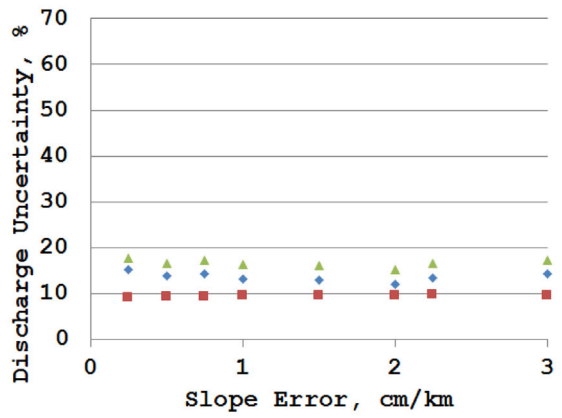scharge error increases significantly up to 62.6%. As illustrated in Figures 8b and 9b, for a height errors above 15 cm the uncertainty due to observation errors becomes greater than the uncertainty due to (n, A_0).

The identification of discharge with Manning equation is relatively insensitive to slope errors (Figure 8d). The overall discharge uncertainty lies between 15% and 18% for slope errors ranging from 0.25 to 3 cm/km. Note that the free surface slope is rather high for the Garonne River ranging from about 60 to 120 cm/km. Thus, measurement errors are generally less than 5% of the actual value. The observation errors (red squares) are a relatively small part compared to the error due to (n, A_0) (blue diamonds). From Figure 9d, it is clear that the uncertainty on Q is not varying as a function of slope error over the studied variation range. A larger part of the uncertainty is due to the uncertainty on (n, A_0) than the uncertainty on observations.

The sensitivity of discharge uncertainty to width error is illustrated in Figures 8f and 9f. The uncertainty due to observation errors increases steadily and for width error larger than 15% it becomes greater than errors in roughness and bathymetry for the Garonne River. The identification can be significantly affected by width errors, for instance, an error of 25% in width will lead to approximately 50% discharge error. The uncertainty is also significantly dominated by observation errors above 15% width errors.

4.3. Sacramento River Versus Garonne River

While discharge estimation accuracy is similar for the Sacramento and Garonne Rivers, results from previous sections illustrate some contrasts concerning the discharge error budget and the sensitivity to AirSWOT
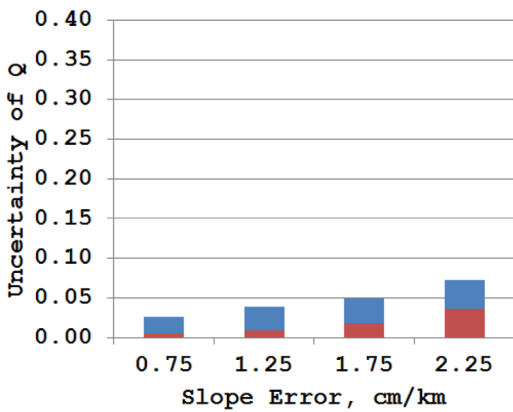
Figure 8. Sensitivity of the algorithm accuracy to the AirSWOT height, width, and slope error for (left) Sacramento River and (right) Garonne River.
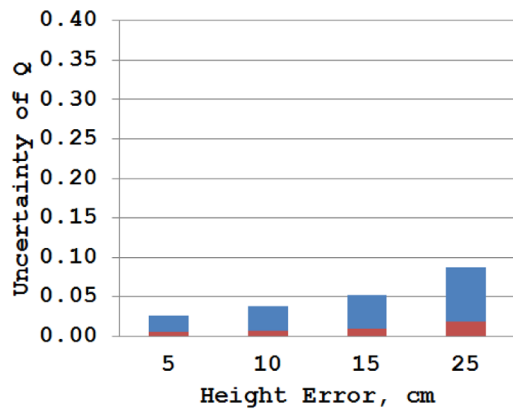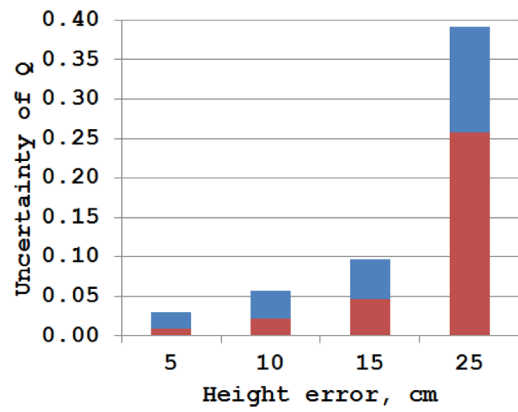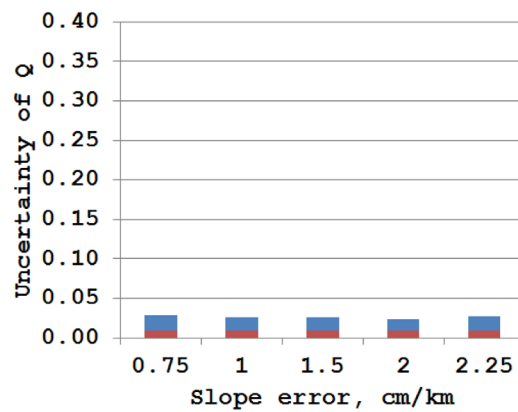
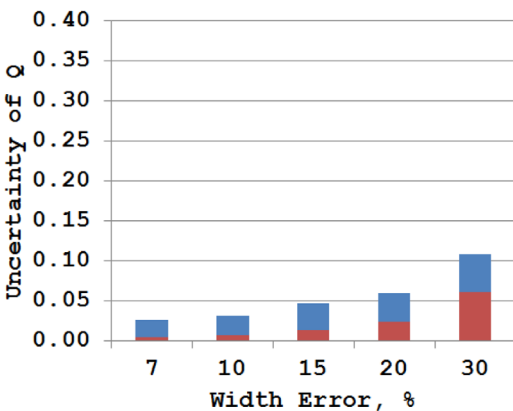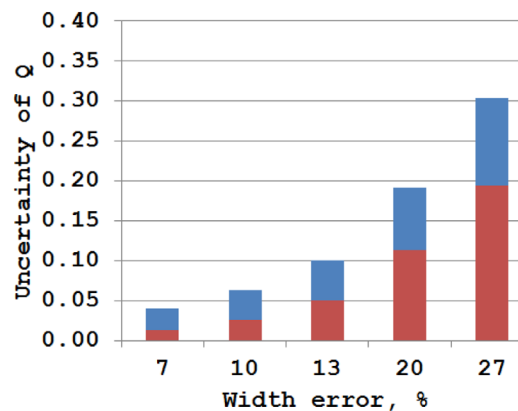**Figure 9.** Sensitivity of the algorithm accuracy to the uncertainties in AirSWOT observations of height, width, and slope for (left) Sacramento River and (right) Garonne River.

measurement errors that can be explained by the different hydraulic characteristics of these systems (summarized in Table 1).

The Sacramento River presents lower slopes and larger relative slope range while the Garonne River shows lower height and width range. Results show that the primary source of error of discharge estimation at Sacramento River is the unknown bathymetry and roughness, while the slope error is the most important observation error (Figure 6). On the other hand, AirSWOT measurement errors showed to be more important for the Garonne River, especially the ones related to the estimation of cross-sectional flow area, i.e., errors in h and w. As the Sacramento River presents larger variability of hydraulic variables, its measurement errors have a lower impact, as demonstrated in the sensitivity analyses. But as river slope is smaller, any error on this variable plays a significant role. In contrast, the hydraulic variables range to a lower extent at the Garonne River and measurement errors have more impact on discharge estimation.

5. Conclusions

This paper presented an improved algorithm to estimate discharge from river height, width, and slope SWOT-like measurements. It uses a Bayesian MCMC approach to infer "the best" estimates of river bathymetry, roughness, and discharge, given the SWOT observables. The method is built based on *Durand et al.* [2014] work and advances previous research by dealing with uncertain width observations, and applying Kalman filter to improve an accuracy of the discharge final estimates. A formal approach to access the discharge error budget, i.e. the sources of discharge errors, is also presented.

The discharge algorithm was run for two rivers (i.e., the Sacramento River and Garonne River) with different characteristics using synthetic AirSWOT measurements. The algorithm was also evaluated using simulated SWOT measurements for the Sacramento River. The main conclusions from our experiments are: (1) The proposed algorithm successfully recovered river bathymetry and roughness and estimated discharge with relative RMSE of 9–15% and uncertainty of 16–17% from AirSWOT measurements; the algorithm also yielded a discharge RMSE of 15% with 16.2% uncertainty from SWOT scenario; (2) it was possible to get satisfactory discharge estimated with several different bathymetry and roughness pairs, and the retrieved values should be interpreted as effective parameters; (3) the proposed Kalman filter method to lead to improved discharge estimates; (4) the principal source of discharge errors was the a priori uncertainty of bathymetry and roughness parameters, but rivers with low temporal variability in hydraulic observables may be more sensitive to measurement errors; and (5) rivers with different characteristics may present different sensitivity to measurement errors. An important finding was that even without slope variability, the discharge on the Garonne River could still be estimated. This overturns the finding of *Durand et al.* [2010a] that slope variability is a prerequisite to ability to estimating discharge. Thus, these results suggest that co-variability in width and height is adequate to calculate discharge from SWOT-like measurements. While future work should still seek for improvements on discharge estimation methods and evaluations under several other conditions (e.g. braided rivers, controlled rivers, etc.), efforts to reduce uncertainty of prior river bathymetry and roughness are also encouraged.

References

Alsdorf, D. E., E. Rodríguez, and D. P. Lettenmaier (2007), Measuring surface water from space, *Rev. Geophys.*, *45*, RG2002, doi:10.1029/2006RG000197.

Andreadis, K. M., E. A. Clark, D. P. Lettenmaier, and D. E. Alsdorf (2007), Prospects for river discharge and depth estimation through assimilation of swath-altimetry into a raster-based hydrodynamics model, *Geophys. Res. Lett.*, *34*, L10403, doi:10.1029/2007GL029721.

Bates, P.D., M. D. Wilson, M. S. Horritt, D. C. Mason, N. Holden, and A. Currie (2006), Reach scale floodplain inundation dynamics observed using airborne synthetic aperture radar imagery: Data analysis and modeling, *J. Hydrol. 328*, 306–318.

Benke, A. and C. Cushing (2005), Rivers of North America, pp. 375–424, Elsevier Academic Press, Burlington, Mass.

Biancamaria, S., M. Durand, K. M. Andreadis, P. D. Bates, A. Boone, N. M. Mognard, E. Rodríguez, D. E. Alsdorf, D. P. Lettenmaier, and E. A. Clark (2011), Assimilation of virtual wide swath altimetry to improve Arctic river modeling, *Remote Sens. Environ. 115*, 373–381.

Bjerklie, D. M., D. Moller, L. C. Smith, and S. L. Dingman (2005), Estimating discharge in rivers using remotely sensed hydraulic information, *J. Hydrol. 309* (2005), 191–209.

Durand, M., K. M. Andreadis, D. E. Alsdorf, D. P. Lettenmaier, D. Moller, and M. Wilson (2008), Estimation of bathymetric depth and slope from data assimilation of swath altimetry into a hydrodynamic model, *Geophys. Res. Lett.*, *35*, L20401, doi:10.1029/2008GL034150.

Durand, M., E. Rodríguez, D. E. Alsdorf, and E. Trigg (2010a), Estimating river depth from remote sensing swath interferometry measurements of river height, slope, and width, *IEEE J. Sel. Top. Appl. Earth Obs. Remote Sens. 3*(1), 20–31.

Durand, M., L. Fu, D. P. Lettenmaier, D. E. Alsdorf, E. Rodríguez, and D. Esteban-Fernandez (2010b), The Surface Water and Ocean Topography Mission: Observing Terrestrial Surface Water and Oceanic Submesoscale Eddies, *Proc. IEEE. 98*(5), 766–779.

Durand, M., J. Neal, E. Rodríguez, K. M. Andreadis, L. C. Smith, and Y. Yoon (2014), Estimating reach-averaged discharge for the River Severn from measurements of river water surface elevation and slope, *J. Hydrol. 511*(2014), 92–104.

Garambois, P.-A and J. Monnier (2015), Inference of river properties from remotely sensed observations of water surface, *Adv. Water Resour.*, *79*, 103–120, doi:10.1016/j.advwatres.2015.02.007.

Gelman, A., G. O. Roberts, and W. R. Gilks (1996), Efficient Metropolis jumping rules, *Bayesian Stat.*, *5*, 599–607.

Gleason, C. J. and L. C. Smith (2014), Toward Global Mapping of River Discharge Using Satellite Images and at-Many-Stations Hydraulic Geometry, *Proc. Natl. Acad. Sci.*, *111*(13), 4788–4791, doi:10.1073/pnas.1317606111.

Gleason, C. J., L. C. Smith, and J. Lee (2014), Retrieval of river discharge solely from satellite imagery and at-many-stations hydraulic geometry: Sensitivity to river form and optimization parameters, *Water Resour. Res.*, *50*, 9604–9619, doi:10.1002/2014WR016109.

Kouraev A.V., E. A. Zakharova, O. Samain, N. M. Mognard, and A. Cazenave (2004), Ob' river discharge from TOPEX/Poseidon satellite altimetry (1992–2002), *Remote Sens. Environ. 93*(1-2), 238–245.

Larnier, K. (2010). Modélisation thermohydraulique d'un tronçon de Garonne en lien avec l'habitat piscicole: Approches statistique et déterministe, PhD thesis, Univ. of Toulouse, Toulouse, France.

LeFavour, G., and D. Alsdorf (2005), Water slope and discharge in the Amazon River estimated using the shuttle radar topography mission digital elevation model, *Geophys. Res. Lett.*, *32*, L17404, doi:10.1029/2005GL023836.

Mersel, M. K., L. C. Smith, K. M. Andreadis, and M. T. Durand (2013), Estimation of river depth from remotely sensed hydraulic relationships, *Water Resour. Res.*, *49*, 3165–3179, doi:10.1002/wrcr.20176

Metropolis, N., A. W. Rosenbluth, M. N. Rosenbluth, A. Teller, and H. Teller (1953), Equations of state calculations by fast computing machines, *J. Chem. Phys. 21*, 1087–1091.

Moller, D., and J. Carswell (2009), *The Ka-band SWOT Phenomenology Airborne Radar (KaSPAR): A Novel Multi-baseline Interferometer for SWOT Characterization, Calibration and Validation*, Remote Sens. Solution, Inc. Monrovia, Calif. [Available at http://www.remotesensingsolutions.com/whitepapers/KaSPAR_WhitePaper.pdf, last accessed September 2015.]

Neal, J. C., G. Schumann, P. D. Bates, W. Buytaert, P. Matgen, and F. Pappenberger (2009), A data assimilation approach to discharge from space, *Hydrol. Process.*, *23*, 3641–3649.

Paiva, R. C. D., M. T. Durand, and F. Hossain (2015), Spatiotemporal interpolation of discharge across a river network by using synthetic SWOT satellite data, *Water Resour. Res.*, *51*, 430–449, doi:10.1002/2014WR015618.

Pavelsky, T. M., M. T. Durand, K. Andreadis, R. E. Beighley, R. C. D. Paiva, G. H. Allen, and Z. F. Miller (2014), Assessing the potential global extent of SWOT river discharge observations, *J. Hydrol.*, *519*, 1516–1525, doi:10.1016/j.jhydrol.2014.08.044

Rodríguez, E. (2015), SWOT science requirements document, NASA JPL document, Initial release. [Available at https://swot.jpl.nasa.gov/files/swot/SRD_021215.pdf, last accessed December 2015.]

Simeoni-Sauvage, S. (1999), Modélisation hydro biogéochimique de la Garonne à l'étiage estival: cas de l'azote entre Toulouse et Agen (120 kilomètres), PhD thesis, Univ. of Toulouse, Toulouse, France.

Smith, L. C., B. L. Isacks, A. L. Bloom, and A. B. Murray (1996), Estimation of discharge from three braided rivers using synthetic aperture radar satellite imagery: Potential application to ungaged basins, *Water Resour. Res.*, *32*(7), 2021–2034, doi:10.1029/96WR00752.

Yoon, Y., and E. Beighley (2015), Simulating streamflow on regulated rivers using characteristic reservoir storage patterns derived from synthetic remote sensing data, *Hydrol. Process.*, *29*, 2014–2026, doi: 10.1002/hyp.10342.

Yoon, Y., M. Durand, C. J. Merry, E. A. Clark, K. M. Andreadis, and D. E. Alsdorf (2012), Estimating river bathymetry from data assimilation of synthetic SWOT measurements, *J. Hydrol.*, *464–465*, 363–375, doi:10.1016/j.jhydrol.2012.07.028.

Yoon, Y., M. Durand, C. J. Merry, and E. Rodriguez (2013). Improving Temporal Coverage of the SWOT Mission Using Spatiotemporal Kriging, *IEEE J. Sel. Top. Appl. Earth Obs. Remote Sens.*, *6*, 1719–1729, doi:10.1109/JSTARS.2013.2257697.

Yoon, Y., E. Beighley, H. Lee, T. Pavelsky, and G. Allen (2015), Estimating flood discharges in reservoir-regulated river basins by integrating synthetic SWOT satellite observations and hydrologic modeling, *J. Hydrol. Eng.*, doi:10.1061/(ASCE)HE.1943-5584.0001320, in press.